Fracture development within a stratovolcano: the Karaha–Telaga Bodas geothermal field, Java volcanic arc

M. NEMČOK[1], J. N. MOORE[1], R. ALLIS[2] & J. McCULLOCH[3]

[1]*Energy and Geoscience Institute, University of Utah, 423 Wakara Way, Suite 300, Salt Lake City, UT 84108, USA (e-mail: mnemcok@egi.utah.edu)*
[2]*Utah Geological Survey, 1594 W North Temple Street, Suite 3110, Salt Lake City, UT 84116, USA*
[3]*Coso Operating Company, LLC, 900 N. Heritage Drive, Ridgecrest, CA 93555, USA*

Abstract: Karaha–Telaga Bodas, a vapour-dominated geothermal system located in an active volcano in western Java, is penetrated by more than two dozen deep geothermal wells reaching depths of 3 km. Detailed paragenetic and fluid-inclusion studies from over 1000 natural fractures define the liquid-dominated, transitional and vapour-dominated stages in the evolution of this system.

The liquid-dominated stage was initiated by a shallow magma intrusion into the base of the volcanic cone. Lava and pyroclastic flows capped a geothermal system. The uppermost andesite flows were only weakly fractured due to the insulating effect of the intervening altered pyroclastics, which absorbed the deformation. Shear and tensile fractures that developed were filled with carbonates at shallow depths, and by quartz, epidote and actinolite at depths and temperatures over 1 km and 300°C. The system underwent numerous cycles of overpressuring, documented by subhorizontal tensile fractures, anastomosing tensile fracture patterns and implosion breccias.

The development of the liquid system was interrupted by a catastrophic drop in fluid pressures. As the fluids boiled in response to this pressure drop, chalcedony and quartz were selectively deposited in fractures that had the largest apertures and steep dips. The orientations of these fractures indicate that the escaping overpressured fluids used the shortest possible paths to the surface.

Vapour-dominated conditions were initiated at this time within a vertical chimney overlying the still hot intrusion. As pressures declined, these conditions spread outward to form the marginal vapour-dominated region encountered in the drill holes. Downward migration of the chimney, accompanied by growth of the marginal vapour-dominated regime, occurred as the intrusion cooled and the brittle–ductile transition migrated to greater depths. As the liquids boiled off, condensate that formed at the top of the vapour-dominated zone percolated downward and low-salinity meteoric water entered the marginal parts of the system. Calcite, anhydrite and fluorite precipitated in fractures on heating. Progressive sealing of the fractures resulted in the downward migration of the cap rock. In response to decreased pore pressure in the expanding vapour zone, walls of the fracture system within the vapour-dominated reservoir progressively collapsed. It left only residual permeability in the remaining fracture volume, with apertures supported only by asperities or propping breccia. In places where normal stresses acting on the fracture walls exceeded the compressive strength of the wall rock, the fractures have completely collapsed.

Fractures within the present-day cap rock include strike- and oblique-slip faults, normal faults and tensile fractures, all controlled by a strike-slip stress regime. The reservoir is characterized by normal faults and tensile fractures controlled by a normal-fault stress regime. The fractures show no evidence that the orientation of the stress field has changed since fracture propagation began.

Fluid migration in the lava and pyroclastic flows is controlled by fractures. Matrix permeability controls fluid flow in the sedimentary sections of the reservoir. Productive fractures are typically roughly perpendicular to the minimum compressive stress, σ_3, and are prone to slip and dilation within the modern stress regime.

This chapter introduces a study of the fracture development in an andesite-hosted geothermal system at Karaha–Telaga Bodas, Indonesia. It is based on the fracture logging from core, interpretation of Electrical Micro Imaging (EMI) and Formation Micro Scanner (FMS) images from deep geothermal production wells, and mineralogical and petrological work. Individual goals include:

- determination of whether far-field stresses changed among different fracture events;
- determination of fracture orientations and kinematics;
- determination of fracture seal/conduit properties;
- determination of the relative succession of fractures.

Existing studies of fracturing in thermal–elastic systems

During the past few decades, fracture studies have focused on various aspects of thermal–elastic

From: COSGROVE, J. W. & ENGELDER, T. (eds) 2004. *The Initiation, Propagation, and Arrest of Joints and Other Fractures*. Geological Society, London, Special Publications, **231**, 223–242. 0305-8719/04/$15

systems. Studies of potential nuclear waste repositories resulted in the formulation of governing equations of processes that link thermal gradients, hydrological flow and mechanical deformation in fractured rock (e.g. Tsang 1999, and references therein). Seismologists and petrophysicists have recognized that the bottoming of earthquakes related to the transition from brittle to plastic behaviour occurs at very shallow depths beneath active high-temperature geothermal fields such as The Geysers and the Imperial Valley, California (Gilpin & Lee 1978; Majer & McEvilly 1979; Sibson 1982). Geothermal deep wells drilled to depths where temperatures exceeded 370–400 °C have encountered a host rock with very little permeability and pore fluid pressures significantly higher than hydrostatic (e.g. Cappetti *et al.* 1985; Ferrara *et al.* 1985; Fournier 1991). Epithermal ore deposit studies have provided the evidence for the narrow transition from an overlying environment with hydrostatically pressured fluids to the underlying almost lithostatically pressured regime (e.g. Hedenquist *et al.* 1998; Fournier 1999). Conceptual models described this transition as the brittle–ductile transition (e.g. Fournier 1999). According to these models, magmatic fluids initially trapped in overpressured ductile rocks can escape into overlying hydrostatically pressured brittle rocks when they are released by brittle fracturing (Fournier 1999). Inside the brittle section with hydrostatic regime, these fluids interact with the dominating meteoric fluids. Owing to the progressive deepening of the brittle–ductile transition with cooling of the geothermal system, the release of the trapped magmatic fluids is understood as transient (e.g. Fournier 1999). Apart from cooling, fluid release from the ductile zone can be caused by increasing the pressure of the trapped fluid or extremely rapid stress release.

Mass-balance calculations of porphyry ore deposits, such as the Pine Grove molybdenum deposit in Colorado, demonstrate that large amounts of fluid from the underlying magmatic reservoir can be released through small intrusions (Keith & Shanks 1988). Further research on this subject resulted in an improved understanding of fluid transport in a convecting magma column (Shinohara *et al.* 1995). Recent experiments document that the mechanical properties of cooling intrusions related to stratovolcanoes depend on the melt fraction and transport properties (e.g. Shaw 1969; Murase & McBirney 1973; Renner *et al.* 2000). Other studies have shown the importance of fluid-assisted deformation in deep high-temperature environments (e.g. Blanpied *et al.* 1995), formulated fracture criteria and conditions for the overlying hydrostatically pressured environment (e.g. Secor 1965; Etheridge 1983; Sibson 1996), described the role of fluids in brittle faulting (e.g. Byerlee 1993; Malin 1994; Miller *et al.* 1996; Hardebeck & Hauksson 1999), and documented a relationship between faults most likely to slip under modern stress and those likely to be conductive to fluids (e.g. Barton *et al.* 1995).

The literature addressing various subjects related to fracturing in a complex thermal–elastic setting is large and diverse; many papers deal with specific aspects of fracturing in this setting. They frequently lack data from well-explored present-day geothermal systems. In this chapter, we describe the fracture development of the Karaha–Telaga Bodas geothermal field of west Java, which is associated with an active stratovolcanic system. Karaha–Telaga Bodas is the most extensively cored volcanic-hosted active geothermal system in the world. The system is shallow and hot. Its wells reach the brittle–ductile transition, and contain pertinent temperature and pressure information. Maximum present-day temperatures are about 350 °C. A relatively simple thermal and structural history of the system makes it especially suitable as a natural laboratory for studying fracturing in a complex thermal–elastic setting.

Geological setting of the Karaha–Telaga Bodas geothermal field

Karaha–Telaga Bodas is one of several large geothermal systems occurring in west Java, Indonesia (Fig. 1a). This newly discovered geothermal field is situated within a N–S-trending andesitic ridge, which is perpendicular to the modern-day minimum principal stress (Nemčok *et al.* 2001). Galunggung Volcano, located at the southern end of the ridge, erupted five times between 1822 and 1984. Telaga Bodas, a shallow acid lake, is located approximately 5.2 km north of the crater at Kawah Galunggung. This ESE-facing horseshoe-shaped crater is believed to have formed 4200 years ago (Katili & Sudradjat 1984) in response to the formation of a large debris avalanche (Brantley & Glicken 1986). Deep drilling by the Karaha–Bodas Co. LLC in 1995–1997 defined a large, partially vapour-dominated system. This system consists of a locally thick cap rock characterized by steep temperature gradients and low permeabilities, an underlying vapour-dominated region that extends to depths below sea level, and a deep liquid-dominated region with measured temperatures up to 350 °C (Fig. 1b)(Allis *et al.* 2000). The vapour-dominated regime extends laterally for at least 10 km; and it is characterized by subhydrostatic pressures and low-temperature gradients.

The geothermal system is developed mainly in andesite–basaltic andesite lava flows, pyroclastics, epiclastic flows, tuffs and sediments, all deposited during the last 1.75 Ma (Katili & Sudradjat 1984; Ganda *et al.* 1985). Granodiorite has been encountered in several of the wells at depths of about 3 km, and locally mafic dykes are present. The granodior-

ite may provide the heat that drives the geothermal system.

Despite the large size of the system and the high measured temperatures, there are few surficial manifestations. These occur mainly at the southern and northern ends of the prospect. Features at the southern end include Telaga Bodas fumaroles (Kawah Saat), and springs that discharge acid sulphate–chloride (pHs to <2) and neutral pH bicarbonate waters. Surface manifestations at the northern end consist mainly of fumarolic activity and associated argillic alteration. $^{3}He/^{4}He$ ratios of 7.1–7.7 Ra indicate the presence of magmatic gas contributions in springs and fumaroles at both the Telaga Bodas (southern) and Karaha (northern) ends of the field.

The deep reservoir fluids appear to be mainly meteoric in origin with locally appreciable magmatic contributions (Powell *et al.* 2001). These deep liquids have relatively low salinities of 1–2 wt% total dissolved solids, and variable chloride/boron ratios of 2.4–20, which imply that the condensation of steam and gases may play an important role in controlling their chemistries. Shifts in the ^{18}O isotope compositions of the waters away from the meteoric water line suggest that a magmatic influence is strongest at the southern end of the field

The results of our investigations, which are described below, indicate that fluid flow within the geothermal system is predominantly fracture-controlled, although locally matrix permeabilities in the sedimentary units are high enough to contribute to fluid production. Only two faults with NW–SE strikes, one fault with a WNW–ESE strike and one with an ENE–WSW strike have been identified by surface geological mapping (Budhitrisna 1986) because of the extensive vegetation and young ash cover. However, numerous faults have been identified by Landsat image mapping (Nemčok *et al.* 2001). Of these faults 53% have strikes ranging between 102°–158° and 282°–338°, while the remaining 47% range between 44°–78° and 224°–258°.

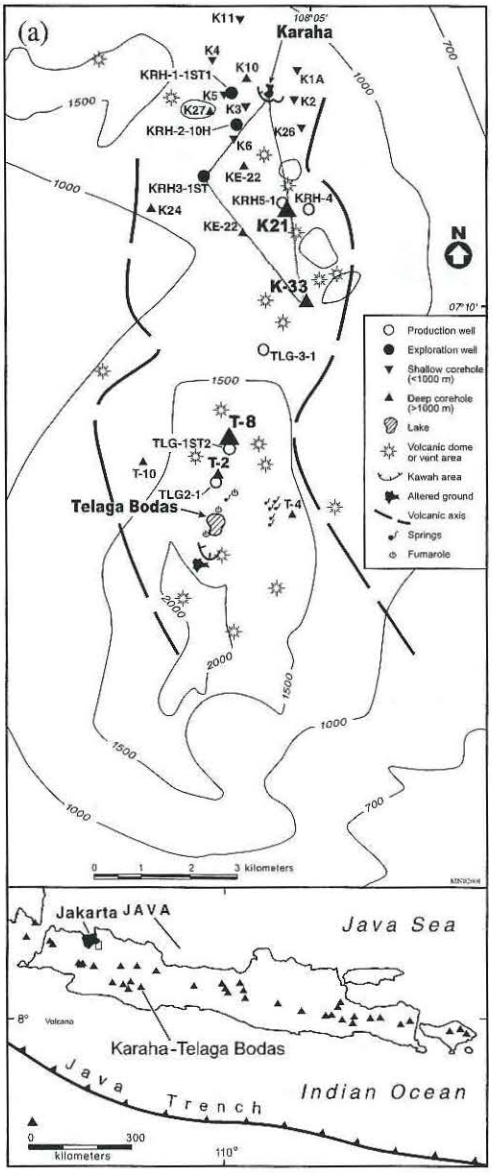

Fig. 1. (**a**) Map of the Karaha–Telaga Bodas geothermal system showing locations of wells and thermal features. Triangles in the inset indicate volcanoes active since 10000 BP. (**b**) North–south cross-section through the Karaha–Telaga Bodas geothermal system with temperatures shown as isotherms in °C, fluid state and spot pore fluid pressure measurements in bars in the highlighted vapour zone (modified from Allis *et al.* 2000). (**c**) Pressure (*P*) and temperature (*T*) trends with depth from corehole K-33. Triangle and triangle/line patterns indicate lava flows and pyro-/epiclastic flows, respectively. Tuff and sediment horizons are in black.

Regional tectonics

The Indonesian island arc system is located at the junction of the Indian, Australian, Pacific and SE Asian plates. Java is characterized by active volcanism and deep earthquakes north of the island under the Java Sea (Hamilton 1974*a*, *b*, 1978). An outer arc, together with a forearc basin, is located south of Java (Hamilton 1974*b*; Baumann 1982). Sumatra is characterized by an outer island arc, a small amount of active volcanism, a lack of deep earthquakes east of the island and a dextral strike-slip component of deformation (Hamilton 1974*a*, 1978). This strike-slip system accommodates the SSW movement of the SE Asian Plate. The Sumatra and Java trenches

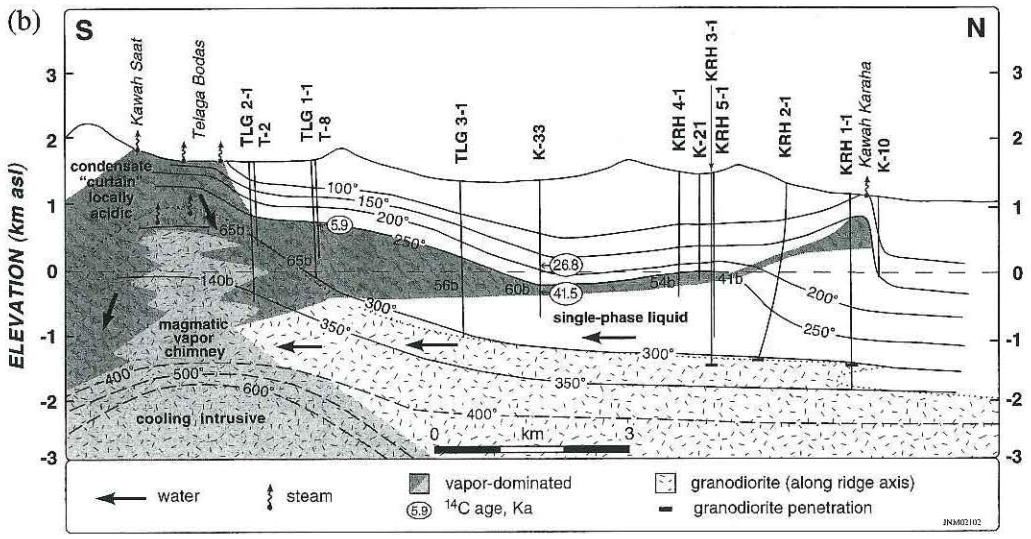

Fig. 1. continued

are zones of northward underthrusting of the Indian Plate.

Reconstruction of plate movements by Hall (1997) suggests that SE Asia was largely recognizable in its present form by 10 Ma, and that the modern-day stress regime was already established by Quaternary time. Since at least 10 Ma, convergence in Sumatra was partitioned into orthogonal subduction and dextral strike-slip motion. The fact that the plate movement vectors have been stable for the last 10 Ma implies that the orientation of the present-day regional stress field (Fig. 2) has been relatively stable throughout the evolution of Karaha–Telaga Bodas geothermal system, which is less than 6000 years old (Bronto 1989; Moore *et al.* 2002). This is an important conclusion because it suggests that the fault kinematics in the geothermal field can be predicted from present-day stress data and fracture geometries. This conclusion is also demonstrated by fracture analysis in corehole K-33 (Table 1), described below.

Local large-scale faults have the following orientations: dip directions of 90°–120° and 270°–300° for normal faults, 20°–40° and 200°–220° for dextral strike-slip faults, 40°–60° and 220°–240° for dextral slightly oblique–slip faults, 60°–90° and 240°–270° for dextral oblique–slip faults, 120°–130° and 300°–310° for sinistral oblique-slip faults, and 130°–150° and 310°–330° for sinistral strike-slip faults (Nemčok *et al.* 2001).

Methods

Fracture orientations and kinematics were studied in three wells, corehole K-33, and two deep production tests, KRH 2-1OH and KRH 3–1ST. Data from the production tests are based on interpretation of electric image logs; data from K-33 are based on detailed logging of the core.

K-33 (Fig. 1a), drilled in the centre of the prospect, was studied in detail. Approximately 500 fractures, which allowed determination of their kinematics, were measured and described (Table 1). These data were compared with temperature and pore fluid pressure distributions in the well to determine the characteristics of producing and sealing fractures. Fracture wall structures have been studied in order to determine any changes in fracture driving stresses. Cross-cutting relationships of various fractures have been recorded in order to determine the relative succession of fractures.

Interpretation of EMI (Haliburton 1995) and FMS (Schlumberger 1992) electric images from wells KRH 2-1OH and KRH 3–1ST (Fig. 1a) was also conducted in order to determine the orientation of the modern principal stresses, fracture orientations and kinematics. Approximately 400 natural fractures of various kinds and orientations and 19 drilling-induced vertical tensile fractures were identified in the reservoir section of well KRH 3–1ST. One hundred and thirty-six natural fractures and 170 drilling-induced borehole breakout fractures were identified in the reservoir section of well KRH 2-1OH. Drilling-induced tensile and borehole breakout fractures were used to constrain the orientation of the principal stresses. These stresses allowed determination of fracture kinematics. Fracture orientation and kinematics data were compared with temperature and pore fluid pressure distributions in both wells to determine the characteristics of producing and sealing fractures.

(c) **DOWNHOLE SUMMARY PLOT, KARAHA COREHOLE K-33**

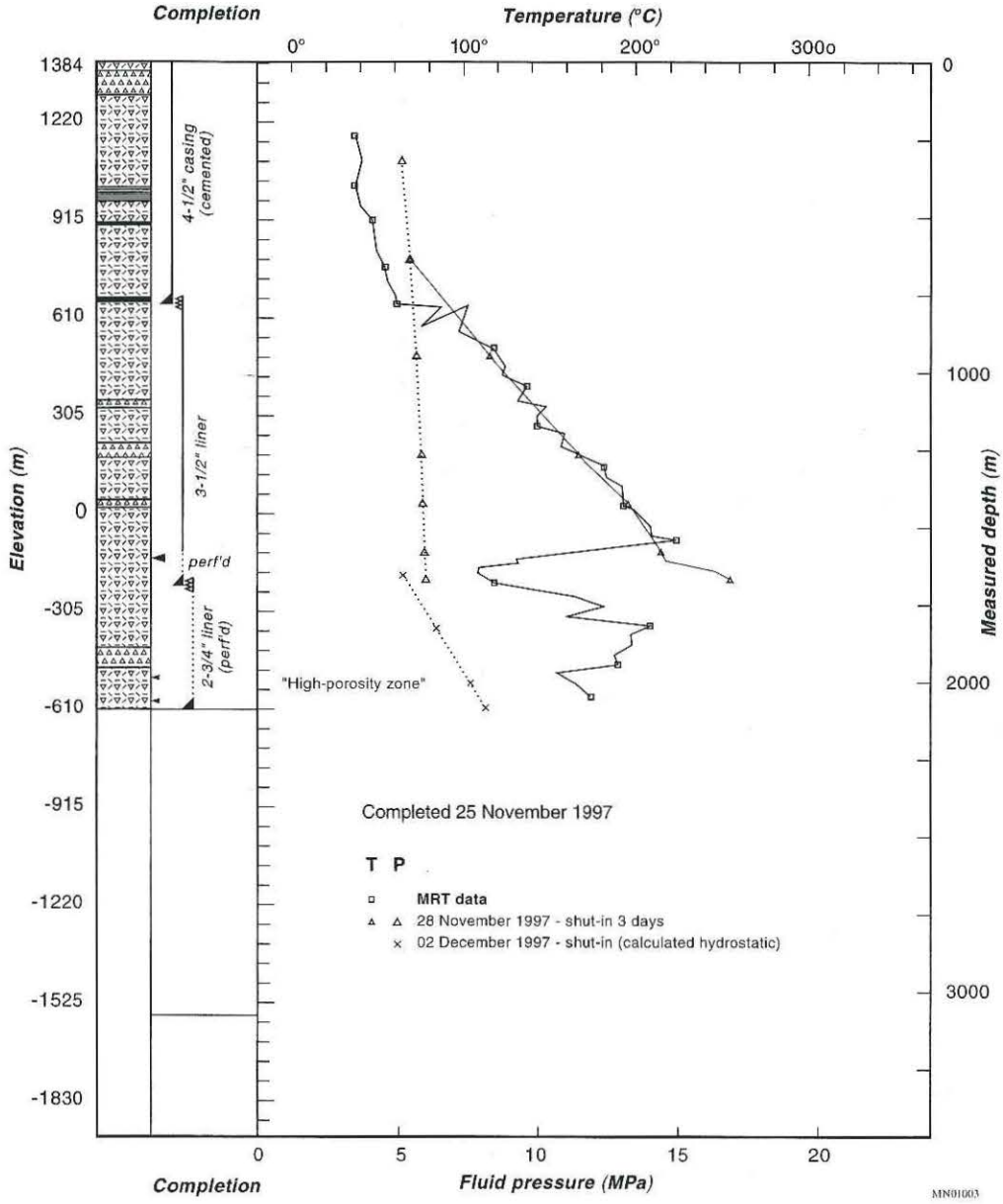

Fig. 1. continued

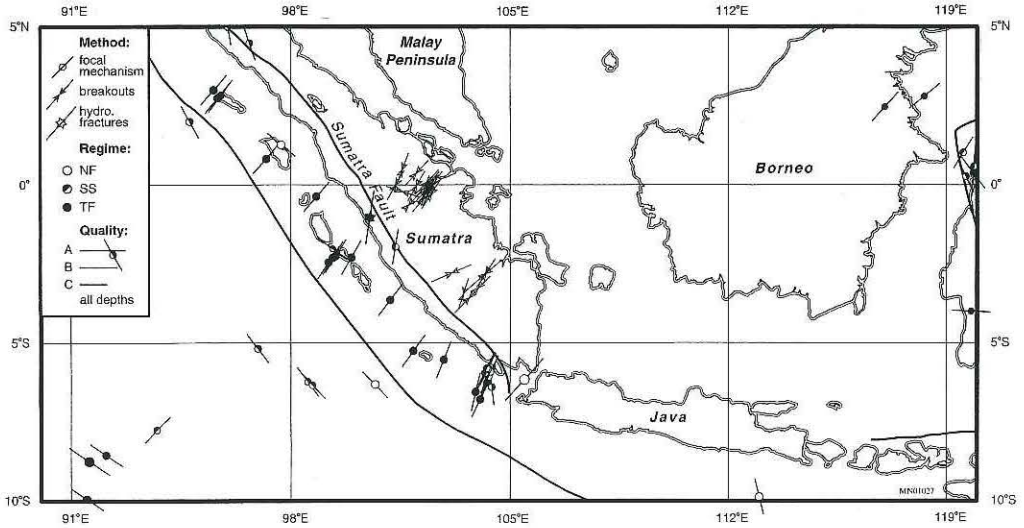

Fig. 2. *In situ* stress data from the Java region taken from the World Stress Map database (modified from Mueller *et al.* 1997). Data are based on focal-mechanism solutions, borehole breakouts and analysis of hydrofracturing results. In the case of focal-mechanism solutions, normal (NF), strike-slip (SS) and thrust (TF) faulting regimes are defined. Data quality, decreasing with the line length, is divided into three categories.

Detailed mineralogical, petrological and fluid-inclusion measurements have been made on coreholes K-33, T-8 and T-2 as part of an on-going study. These measurements provide insight into the sequence of mineralizing events (Allis & Moore 2000; Moore *et al.* 2000, 2001, 2002) and the relative timing of the associated fracturing.

Data

Fracture data from corehole K-33

K-33 was continuously cored from 754.3 to 2018.6 m with excellent recovery. The well encountered the top of the vapour-dominated reservoir at a depth of 1538 m. Temperatures within the reservoir section of the well range from 220 to 256 °C at total depth.

Fracture types occurring in K-33 are listed in Table 1. Normal faults, tensile fractures, sinistral and dextral strike-slip faults, and sinistral and dextral oblique-slip faults with a normal component of displacement are present within the cap rock. They have been controlled by the strike-slip stress regime with horizontal maximum and minimum compressional principal stresses, σ_1 and σ_3, and vertical intermediate stress, σ_2. Trends and plunges of principal stresses determined from well KRH 3–1ST, located just 3.4 km to the NW, are: $\sigma_1 = 188°/0°$, $\sigma_2 = 0°/90°$ and $\sigma_3 = 98°/0°$.

Strike-slip faults are totally missing in the reservoir. Instead, normal faults and tensile fractures are characteristic of the reservoir. They have been controlled by vertical σ_1, and horizontal σ_2 and σ_3. Stress trends and plunges are $\sigma_1 = 0°/90°$, $\sigma_2 = 188°/0°$ and $\sigma_3 = 98°/0°$.

The location of the deepest strike-slip fracture indicates that a boundary between the cap rock strike-slip and reservoir extensional regimes lies at a depth of about 1625 m. Magnitudes of the maximum principal compressional stress σ_1 and intermediate principal compressional stress σ_2 are equal at this depth. This is also the depth where the horizontal σ_1 characteristic of the cap rock changes to a vertical σ_1, which is characteristic for the reservoir.

Magnitudes of vertical σ_2 in the cap rock and vertical σ_1 in the reservoir are given by the relationship:

$$\sigma_V = \rho g h \quad (1)$$

where ρ is the density of overburden, g is the acceleration of gravity and h is the thickness of overburden. The change in horizontal σ_1 and σ_3 within the cap rock and horizontal σ_2 and σ_3 within the reservoir can be approximated by:

$$\Delta\sigma_H = \nu(\rho g \Delta h(1 = \nu)) \quad (2)$$

where ν is Poisson's ratio. This provides a maximum stress value because the fluid pressure can take a proportion of the overburden load (e.g. Rice & Cleary 1976; Mandl 1988; Engelder & Fischer 1994, and references therein).

Table 1. *Fracture types in corehole K-33*

Dip	s cr	s r	s Ttl	os cr	os r	os Ttl	d cr	d r	d Ttl	od cr	od r	od Ttl	n cr	n r	n Ttl	on cr	on r	on Ttl	t cr	t r	t Ttl	D
0	1		1																4	5	9	
5																					0	
10													1		1				2		2	
15																			2		2	
20	1		1	1		1							2		2				1	1	2	
25	2		2				2		2				2		2				5	3	8	
30				1		1	1		1	1		1	2		2	1		1	4	2	6	
35	1		1										3		3				4	3	7	
40	3		3				2		2	1		1	5	1	6	1	1	2	29	5	34	
45	7		7	1		1	1		1				6	1	7	1		1	14	5	19	1
50	7		7	3	1	4	2		2				9	4	13	1	2	3	10	9	19	
55	2		2	2	1	3	3		3				6	1	7	3		3	11	5	16	
60	2		2	2		2	1		1		1	1	8	1	9	3		3	11	10	21	2
65	5		5	1		1	3		3				10		10	3	1	4	18	10	28	
70	4		4	2		2	1		1	1		1	5	1	6	7	1	8	17	6	23	
75	6		6	1		1	3		3				2		2				12	10	22	
80	5		5	4		4	2		2	1		1	4	1	5				2	5	7	
85	2		2	4		4	4		4	2		2	5		5	3		3	38	27	65	
			48			24			25			7			80			28			290	

The number indicates the total number of fractures for each category.
Abbreviations: cr, cap rock; d, dextral strike-slip; D, dyke; n, normal fault; od, oblique dextral strike-slip; on, oblique normal fault; os, oblique sinistral strike-slip; r, reservoir; s, sinistral strike-slip; t, tensile fracture; Ttl, total amount.

These equations allow us to estimate the ratios of magnitudes of principal stresses upwards for the cap rock section, and downwards for the reservoir section from a depth of 1625 m in corehole K-33, where σ_1 equals σ_2 in magnitude. The stress estimate above this depth indicates a strike-slip stress regime with $\sigma_1 \geq \sigma_2 \gg \sigma_3$ in the lower portion of the cap rock as σ_1 magnitude approaches the σ_2 magnitude towards the cap rock–reservoir boundary. The boundary between the strike-slip stress regime and normal fault regime, roughly following the cap rock–reservoir boundary, is indicated by the presence of strike-slip fractures in the cap rock of the corehole K-33, and tensile fractures and normal faults in its reservoir section (Table 1).

Owing to the addition of the overburden load with depth, the strike-slip stress regime typical for the cap rock progressively changes with depth to the extensional stress regime characteristic of the reservoir. Within the reservoir, the σ_1 magnitude departs from the σ_2 magnitude with increasing depth towards $\sigma_1 \gg \sigma_2 \geq \sigma_3$ in the deepest parts of the reservoir.

None of the shear fractures observed in corehole K-33 (Table 1) displays any cross-cutting slip vectors. There is no evidence for the reactivation of tensile fractures as younger shear fractures, or for later tensile reactivation of earlier shear fractures. These observations indicate that the stress field did not change during their propagation; otherwise we would expect to see cross-cutting relationships on some of the more than 1000 fracture walls studied. This observation further supports the conclusion, derived from plate reconstructions of Hall (1997), that the local stress field in the Karaha–Telaga Bodas geothermal field was relatively stable during its development.

The temperature distribution in K-33 (Fig. 1c) indicates that faults and fractures in the cap rock section are sealed and poorly connected, because the dominant mode of heat transfer is by conduction. Figure 1c shows an efficient convective heat transfer in the reservoir section, suggesting that fluid flow occurs within a relatively well-connected fault–fracture system. The temperature–depth curve in the reservoir is perturbed at points where cold drilling fluid enters permeable zones.

Fracture data from well KRH 3–1ST

Well KRH 3–1ST has a measured depth of 3078 m. The top of the reservoir is encountered at a depth of about 1996 m and a temperature of 225 °C. The bottom hole temperature is 334 °C. An EMI log was obtained from 2117 to 3016 m.

The log shows that numerous normal faults/ tensile fractures and dextral strike-slip faults have strikes of 350°–30° and 120°–140°, respectively. The less numerous sinistral oblique-slip, sinistral strike-slip

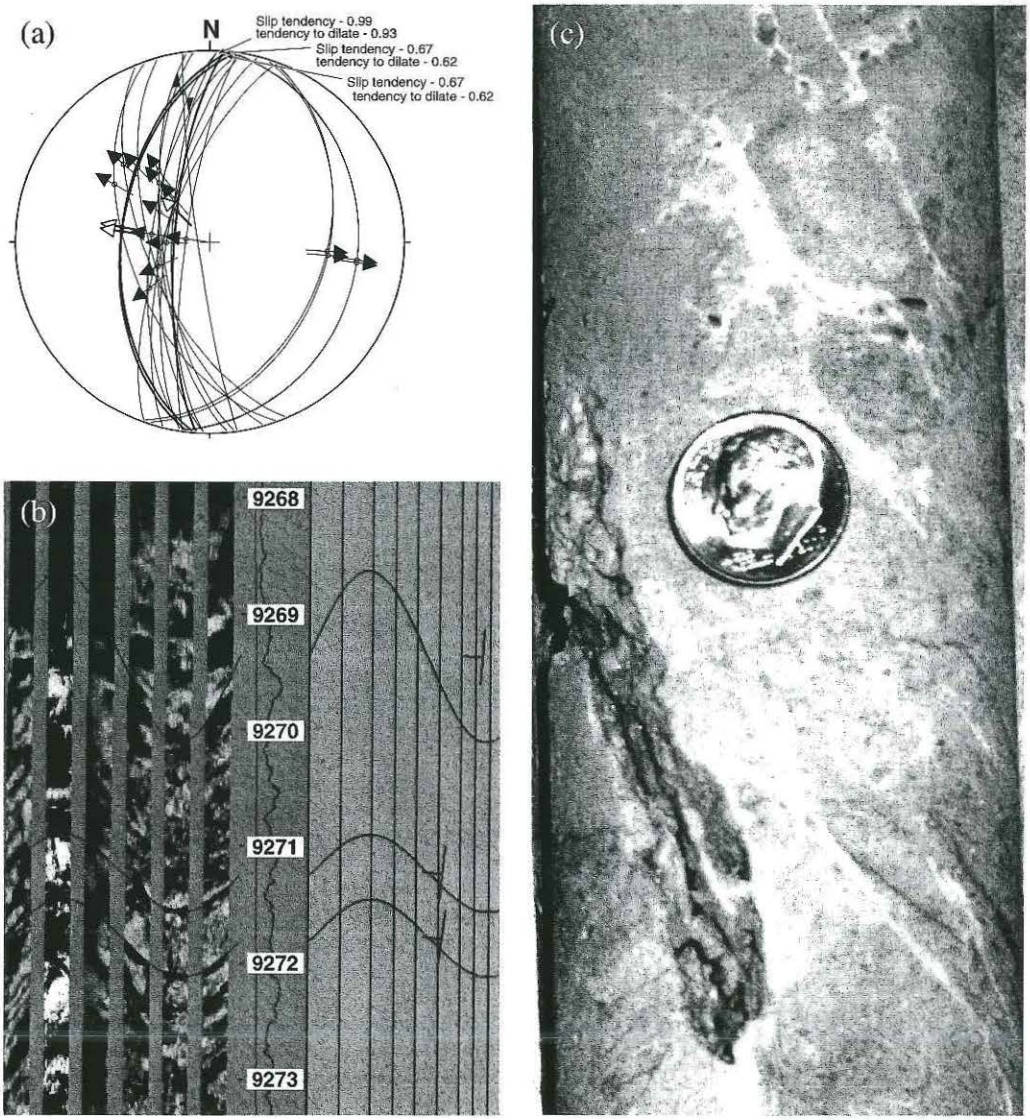

Fig. 3. (**a**) Great circle diagram of shear fracture types in the reservoir depth interval of 2816.1–2858.8 m (9233–9373 ft) in well KRH 3–1ST. Fractures at major fluid entry, documented also by FMS image (b), are in bold. Fracture density in fluid entry surroundings is five fractures per 10 m. Slip tendency is calculated from τ/σ_n, where τ is the shear stress and σ_n is the normal stress. Dilation tendency is calculated from $(\sigma_1 - \sigma_n)/(\sigma_1 - \sigma_3)$, where σ_1 and σ_3 are maximum and minimum principal compressional stresses. Fractures that are very close to being reactivated within the *in situ* stress regime have a slip tendency value near 1, whereas fractures that are unlikely to slip have a value near 0. The maximum and minimum tendency to dilate during slip, denoted by the 'tendency to dilate', is represented by values of 1 and 0, respectively. (**b**) Black and white areas in FMS image indicate conductivity and resistivity, respectively. Black spots located along productive fractures indicate presence of open cavities filled by fluid in dilatant regions. Example of such a fracture from a reservoir section of the corehole K-33 is shown in (**c**).

and dextral oblique-slip faults strike 30°–40°, 50°–70° and 140°–170°, respectively. There are few resistive fracture representations in well KRH 3-1ST. Electrically conductive fracture representations are dominant.

Resistive fracture representations are always associated with non-producing fractures. Their resistive response in the image log is caused by resistive fracture fill, which is interpreted as calcite or quartz, based on a comparison with fills observed in core

from K-33 and their known electric representations (e.g. Adams & Dart 1998).

Conductive fracture representations are associated with both non-producing and producing fractures. EMI representations of some non-productive fractures have apertures at the threshold of detection, i.e. 1 cm; these representations contain large, highly conductive spots that locally coalesce into more extensive patches. Large patches of conductive spots also characterize fractures at minor fluid entries, while major fluid entries are characterized by an increase in the complexity and density of conductive spots within the fractured interval. For example, the densely spotted zone associated with the fluid entry at 2379.3–2380.5 m and the major fluid entry at 2343.3–2344.2 m are imaged as a plethora of fractures that include larger cavities. These cavities have a conductive representation when filled by fluid. Distinct fluid entries can sometimes be located along relatively small fractures, such as the entry at 2827–2828 m (Fig. 3a, b). Some productive fracture images contain sharply defined, highly conductive pull-aparts along the fracture planes. Fractures at all fluid entries, irrespective of fracture densities and the presence or absence of larger cavities, are all characterized by relatively small average apertures. EMI data from KRH 3–1ST also contain broad, highly conductive features that are not related to fluid entries. Their thicknesses range from 0.3 to 1.5 m. These fracture representations always contain numerous resistive spots related to host-rock clasts inside fault cores.

The best productive fractures are tensile fractures and normal faults with strikes typically roughly perpendicular to the minimum compressive stress σ_3, which trends 98°, but exceptions are possible. Such an exception is the fluid entry at 2032 m in KRH 2-1OH related to a fault with a 4.6 m-thick fault core. This dextral oblique-slip fault has a dip direction and dip of 325° and 89°, respectively, and therefore is not 'ideally' oriented. 'Ideally' oriented productive fractures, which have strikes around 8° and steep dips, have a tendency to achieve maximum possible apertures in the modern stress regime.

Calculation of the normal and shear stresses acting upon the fractures, using the equations of Wallace (1951) and Bott (1959), allowed determination of the tendency of the fracture to slip or dilate under the present-day stress regime (Fig. 3a). This calculation shows that among all fractures the majority of productive fractures are most prone to slip and/or dilation under the modern stress. It indicates that the fluid circulation in KRH 3–1ST is clearly affected by the present-day stress regime. All studied productive fractures are located in massive lava and pyroclastic flows, which are more than several metres thick.

The effects of the present-day stress field on reservoir behaviour are illustrated by the fluid entry at 2816.1–2858.8 m (Fig. 3a), which shows the favourable slip and dilation tendencies of productive fractures. The fracture density at this fluid entry is no higher than the average density of five fractures per 10 m determined for the logged portion of the reservoir. Similar fracture densities, no higher than the average, are associated with other production zones. This observation indicates that fracture density cannot be used for distinguishing productive zones from non-productive portions of the reservoir.

The EMI log also indicates that some fluid entries are not associated with fracture zones. These entries are located in moderately conductive, layered, rock sequences, representing epiclastic rocks, tuffs or sedimentary units. A lack of fractures at these entries suggests that matrix permeability controls the fluid flow in these cases.

Fracture timing

Mineralogical relationships. Mineralogical studies of the core and cuttings samples record three major stages in the evolution of the modern geothermal system at Karaha–Telaga Bodas (Moore *et al.* 2001, 2002, 2004). The mineralogical characteristics of these stages are summarized in Table 2.

The earliest hydrothermal activity is represented by pervasive argillic alteration and silicification of the rocks and minor veining. A variety of clay minerals and sheet silicates including smectite, illite–smectite, chlorite–smectite, illite and chlorite were deposited in the veins and wall rocks. These minerals are characteristic of low–moderate temperatures below 250 °C (Henley & Ellis 1983). Younger veins define two parageneses. At depths above 850 m, the veins are dominated by calcite, chlorite, pyrite, or haematite. At greater depths, the veins contain epidote, albite, amphibole and Fe–Cu sulphides. In the deepest explored parts of the system, biotite and clinopyroxene are also present. Amphibole is an important index mineral, occurring in active geothermal systems only at temperatures above 300 °C. In the southern part of the Karaha–Telaga Bodas field, this mineral is locally abundant below 950 m. The widespread occurrence and mineral parageneses of these veins demonstrate that the early geothermal system was liquid dominated and that temperatures were higher in the past than they are today.

Silica deposited as chalcedony and saline fluid inclusions in quartz record the transition from a liquid-dominated stage to a vapour-dominated stage. In the shallow veins, chalcedony replaces the carbonates and fills open spaces. In the deeper veins, chalcedony post-dates the formation of epidote and amphibole (Table 2), occurring mainly as cores of euhedral quartz crystals. Evidence of chalcedony

Table 2. *Relative timing of mineralization events with approximate location*

	Time				
	Penetrative	Early liquid-dominated veins	High-temperature liquid-dominated veins	Transitional veins	Vapour-dominated veins
Near surface	argillic alt. silicification	sericite/chlorite			advanced argillic
Shallow	argillic alt. silicification	sericite/chlorite	chlorite + pyrite calcite/haematite	chalcedony/quartz	calcite + anhydrite
Deep	argillic alt. silicification	quartz sericite/chlorite	epidote + albite + pyrite ± actinolite ± biotite ± clinopyroxene	chalcedony/quartz	anhydrite + pyrite ± wairakite ± calcite ± fluorite

deposition has been found throughout much of the modern geothermal reservoir.

Quartz crystals associated with chalcedony display unusual growth forms. Twinning, curved '*c*'-axes and epitaxial growth are common. No workable fluid inclusions were found in chalcedony. However, fluid inclusions in quartz from depths where chalcedony is present yielded average temperatures of 234 °C, based on 95 inclusions from a depth of 793 m in corehole T-2, and 315 °C, based on 72 inclusions from a depth of 1203 m in corehole T-8. These data and the absence of intervening low-temperature mineral assemblages suggest that chalcedony formed at temperatures above 180 °C. Fournier (1985) has shown that the formation of chalcedony at these temperatures requires extreme supersaturation of silica and rapid decompression of the hydrothermal fluids.

Vapour-rich fluid inclusions, indicative of boiling, are dominant in many of the quartz crystals. Liquid-rich inclusions have yielded homogenization temperatures up to about 350 °C and salinities ranging mainly from 3 wt% NaCl eq. to 24 wt% $NaCl/CaCl_2$ eq. in coreholes T-2 and T-8. Moore *et al.* (2002) have suggested that the high salinities are the result of extreme boiling and concentration of the hydrothermal fluids. In contrast, lower salinity fluids with less than 1–2 wt% NaCl eq. are common in corehole K-33. These fluids are interpreted as steam condensate.

The age of depressurization is constrained by ^{14}C dating of lake beds from a depth of 978 m in corehole T-8 (Moore *et al.* 2002). These sedimentary deposits predate the formation of amphiboles, epidote and chalcedony. Organic carbon in the lake beds has yielded an age of 5910 ± 76 years. Thus, the data suggest that the depressurization is related to an event that is younger than 5910 years old.

The deposition of chalcedony and quartz was followed by anhydrite, calcite, fluorite, pyrite and wairakite (Table 2). Anhydrite, calcite and fluorite have retrograde solubilities and deposit as fluids are heated. The simple parageneses of these veins suggest that mineral deposition occurred in response to the heating of downward-percolating condensate. Fluid inclusions trapped within these minerals record the evolution of the fluids. At shallow depths in T-2, the downward heating is represented by increasing homogenization temperatures from 160 to 225 °C and decreasing salinities due to mineral deposition. At greater depths in T-8, where fluid inclusion homogenization temperatures exceed 225 °C, the apparent salinities increase with temperature, reflecting the boiling off of the fluids. Fluids with salinities as high as 31 wt% NaCl eq. were trapped in anhydrite. Scales of halite, sylvite and Fe-chlorides on the hydrothermal vein minerals demonstrate that the condensate eventually boils off completely within the modern vapour-dominated portion of the system. Thus, the fluid inclusion and mineral data document the drying out of the early liquid-dominated geothermal system.

The low salinities of 1–2 wt% of the present-day reservoir fluids indicate that meteoric waters are presently recharging the geothermal system. However, the occurrence of high $^3He/^4He$ ratios from 7.1 to 7.7 *Ra* throughout the field and large oxygen isotope shifts of the deep liquids suggest the presence of a magmatic contribution to the fluids (Powell *et al.* 2001).

Fractures active during the liquid-dominated stage of geothermal activity. Fractures active during the liquid-dominated stage were coeval with penetrative argillic alteration and silicification. The liquid-dominated system was capped by the upper parts of the stratovolcanic complex, which were affected by argillic alteration. Detailed logging of K-33 indicates that andesite lava flows in the shallow portion of the system have not been extensively fractured, perhaps due to the insulating effect of the intervening altered

Fig. 4. Thin section documenting a penetrative argillic alteration followed by quartz veining.

pyroclastic and epiclastic rocks, which absorbed the deformation. The end result of the argillic alteration in the more porous parts of the section was a significant reduction in the porosity of the cap rock (Fig. 4). Although lava flows in the cap rock were locally fractured, low overall permeabilities are demonstrated by high-temperature gradients indicative of conductive heat transfer (Fig. 1c).

Penetrative fluid events have changed the initial rheological properties of the geothermal system. For example, core from K-33 documents cases of initially low porosity lava and pyroclastic flows of the reservoir that underwent a distinct porosity increase through dissolution of feldspars and only partial fill by later epidote (Fig. 5a). Younger shear fractures in these altered rocks resemble deformation of coarse-grained sandstone (e.g. Antonellini & Aydin 1994). Rocks are not deformed by discrete fractures, which are typical of unaltered lava and pyroclastic flows. They are deformed by densely spaced shear bands.

Later fractures were synchronous with fluid flow. These fluids mainly affected the walls of the fractures with only minor penetration of the wall rocks. The majority of the observed fractures indicates that fluid-assisted failure was dominant. Local exceptions indicate that failure caused by cooling-related stress release was possible (Fig. 6a).

Subhorizontal tensile fractures, opened against the overburden weight, anastomosing tensile fracture patterns, and implosion breccias in the quartz and calcite vein fills are frequent (Fig. 6b). Twenty-three subhorizontal tensile fractures, eight anastomosing tensile fracture patterns and 18 implosion breccias were observed in K-33. They document numerous episodes when local fluid pressures exceeded hydrostatic pressure.

The geothermal system is cut by several faults. Fault cores are usually thinner than 2 m, although one with a thickness of 4.6 m was observed in KRH 2-1OH. Their damage zones are a few times wider than the cores. Fault cores are characterized by

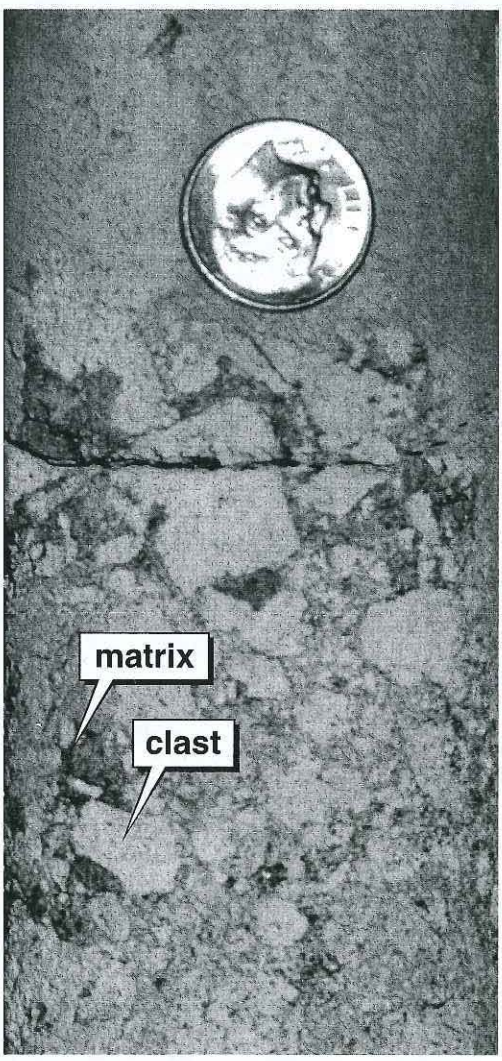

Fig. 5. Example of the penetrative dissolution of feldspars from the pyroclastic flow at a depth of 1750.7 m in the corehole K-33. Note that matrix around the less permeable clasts is preferentially affected. Holes after feldspars are just barely lined by epidote, which did not destroy an enhanced porosity.

cemented or uncemented fault breccia and gouge, which are developed by competing cataclastic flow and fluid-assisted deformation mechanisms. The cataclasis is indicated by frictional wear of clasts (Fig. 6c). Fluid-assisted deformation is indicated by zoned fractures within the damage zones (Fig. 6d). Adjacent parts of the host rock are frequently altered or cemented. There is evidence for hydraulic fracturing that reopened fractures previously cemented by quartz, and for younger cementation by quartz (Fig.

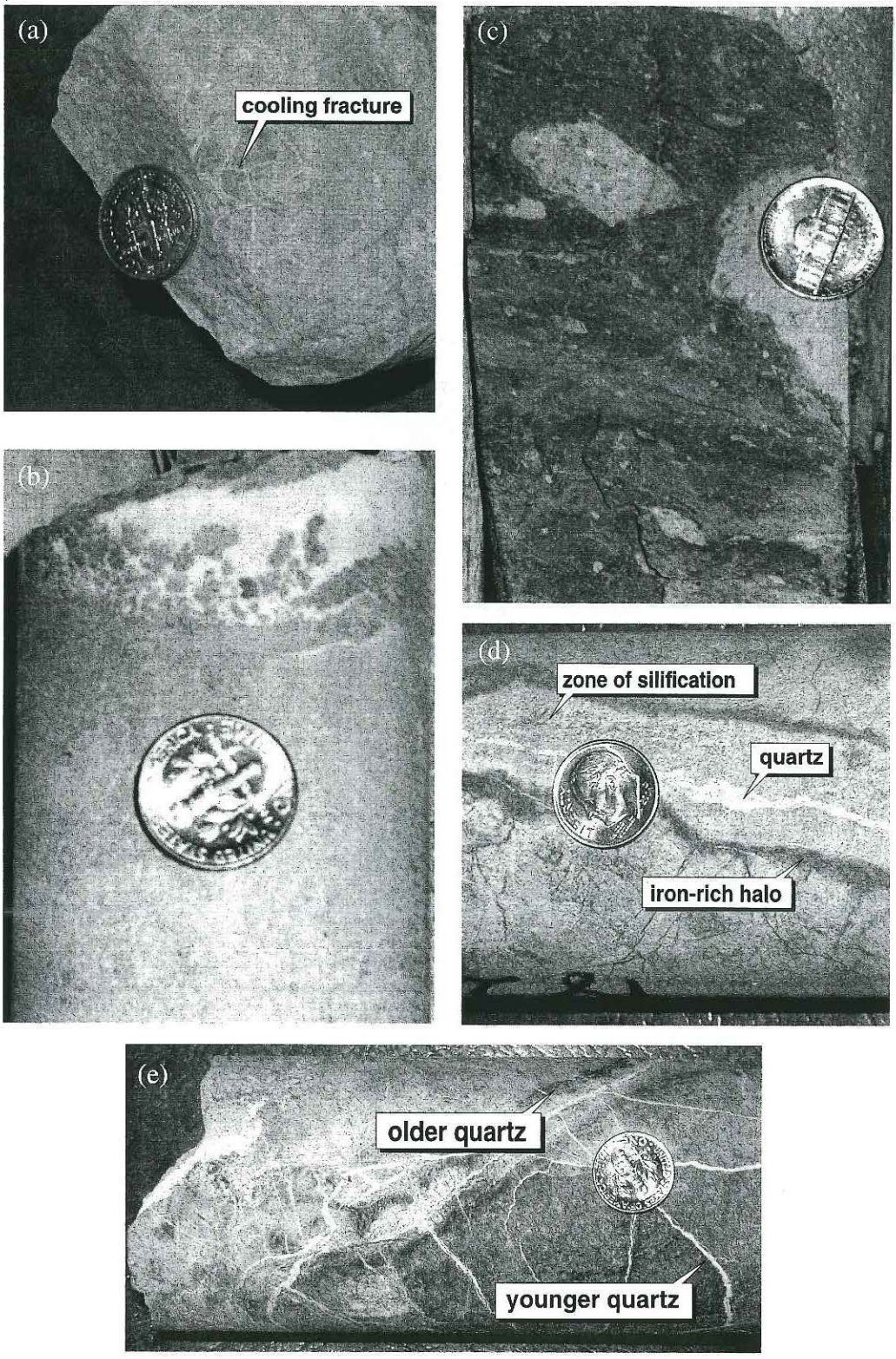
(a)
cooling fracture
(b)
(c)
(d)
zone of silification
quartz
iron-rich halo
(e)
older quartz
younger quartz

6e). Figure 6e shows how the increased pressure of the fluid trapped in the fracture sometimes resulted in small hydraulic fractures propagating away from this fracture into the adjacent host rock in a relatively random fashion, generating temporary storage for fluids, before the main fracture ruptured.

Fractures active during the transition from a liquid- to vapour-dominated stage. Fractures active during this stage are coeval with chalcedony and quartz deposition. They are present at all depths. The chalcedony and associated quartz are found only in tensile fractures and shear fractures with normal displacement. These fractures are characterized by large apertures and steep dips. They were highly prone to slip and dilation. As discussed later, the deposition of chalcedony in these fractures is significant because the chalcedony occupies a unique paragenetic position within the evolution of the hydrothermal system. This position can be correlated across the field. Chalcedony has been found within all of the coreholes over a strike length of over 6 km, and to depths in excess of 2 km. In the shallow portion of the geothermal system, the chalcedony post-dates the calcite associated with the earlier liquid-dominated stage. At greater depths the chalcedony post-dates epidote, amphibole and pyrite deposited by higher temperature liquids (Fig. 7).

Fig. 7. Thin section with a chalcedonic vein in the older actinolite, epidote and pyrite paragenesis within the reservoir at a depth of 1139.5 m in the corehole T-8 (Moore *et al.*, 2000).

Fractures associated with the modern geothermal system. Fractures that were propagated or active after the deposition of chalcedony and quartz are filled by anhydrite, calcite, pyrite and fluorite (Fig. 8a–d).

Fig. 8a shows anhydrite post-dating earlier mineralization in the cap rock. The anhydrite completely fills the only remaining space in a dilatant region of a strike-slip fracture. Figure 8b, c shows anhydrite and calcite that post-date earlier mineralization in the cap rock and reservoir. The calcite completely seals the residual aperture of the pre-existing fracture in Figure 8c. In contrast, the fracture in Figure 8b is only partially sealed by the anhydrite. Figure 8d demonstrates that this stage of calcite deposition post-dates chalcedony in the uppermost part of the reservoir.

The final stage of mineral deposition in these fractures is represented by precipitates of Na-, K- and Fe-chlorides on the mineral surfaces. The high solubilities of these precipitates indicate that no mobile water is present and that essentially complete dry-out of the fractures within the vapour-dominated portion of the system has occurred (Fig. 9). These fractures contain frequent voids. Their apertures are supported by cement bridges, host-rock asperities and propping breccias.

Fig. 6. (**a**) Fracturing related to the release of the residual stress accumulated by cooling of the andesite above the cooling granodiorite intrusion at a depth of 367.6 m in the corehole T-2. Fractures are developed in the altered andesite and filled by quartz. (**b**) Implosion breccia with altered andesite inside a fine calcite matrix at a depth of 1653 m in the corehole K-33. The implosion character can be documented by the fact that boundaries of the neighbour clasts match together. Facts such that there is no deposition of denser clasts on the bottom of the vein and that clasts are not even a little gravitationally sorted indicate a high viscosity of the initial fluid. Such an implosion breccia originates when a rupturation connects areas with higher and lower pore fluid pressure. A pore pressure gradient between such areas is quickly balanced by a rapid fluid flow, and a viscous fluid 'freezes' below the certain threshold flow rate and preserves a pocket of the implosion breccia. (**c**) Fault core from a depth of 1545 m in the corehole K-33 with fault breccia and gouge. The gouge is made by size reduction of andesitic clasts and reaction with fluids rich in silica. Clasts of different sizes are progressively more rounded with smaller clast size, indicating frictional wear. (**d**) Example of the single fracture from a depth of 1827.5 m in the corehole T-2. The fracture is filled by quartz and surrounded by the zone of silicification and iron-rich halo, documenting that silica-rich fluids flowing along the fracture also altered the adjacent portion of the host rock. (**e**) Earlier fracture reopened by hydraulic fracturing from a depth of 389 m in the corehole T-2. Earlier fracture was filled by grey quartz, reopened by hydraulic fracturing and filled by white quartz. Note the small hydraulic fractures filled by white quartz fed by the main hydraulic fracture. They are propagated in a seemingly random manner into the adjacent host rock, generating storage for overpressured fluid.

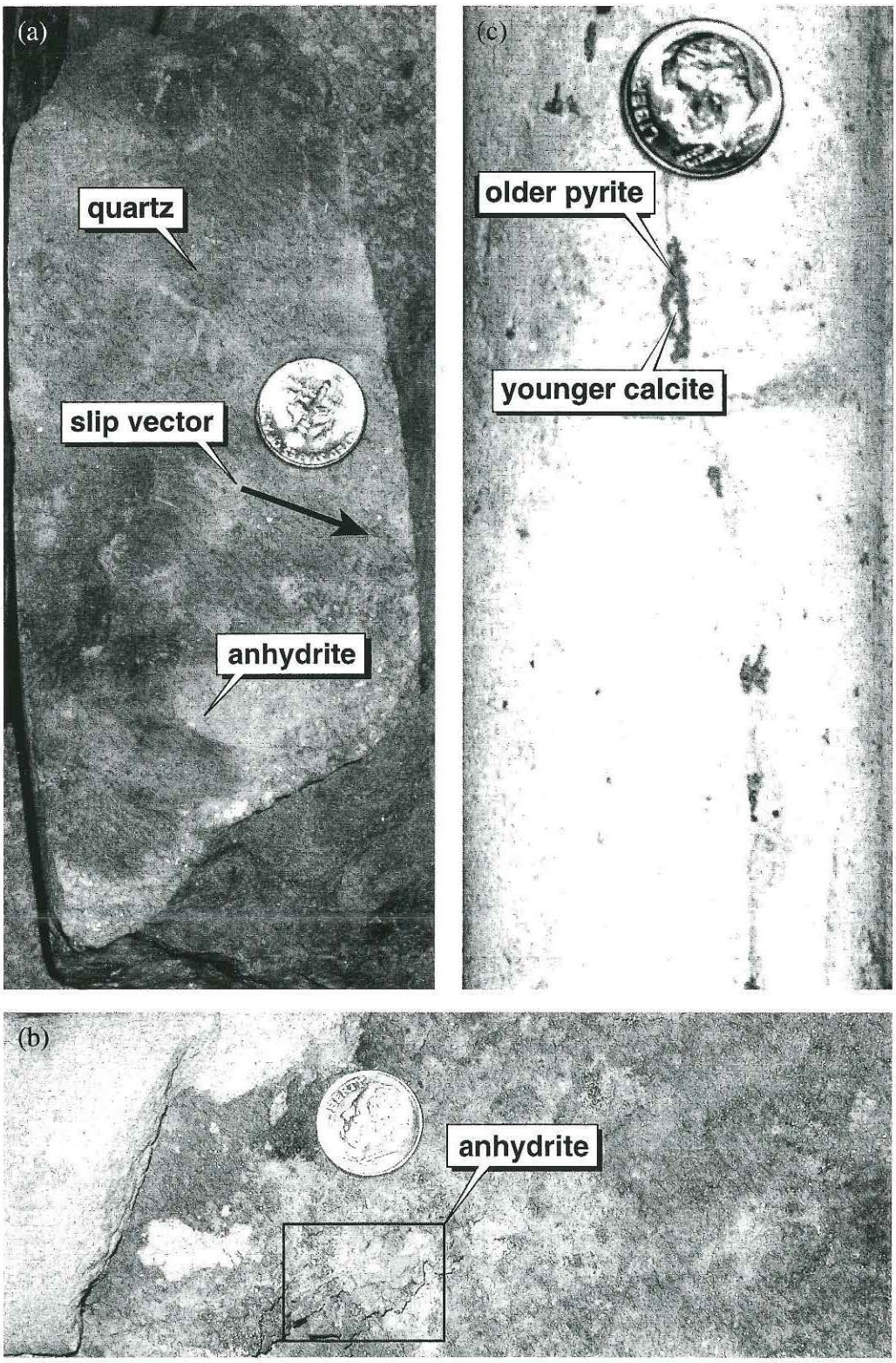
(a)
quartz
slip vector
anhydrite
(c)
older pyrite
younger calcite
(b)
anhydrite

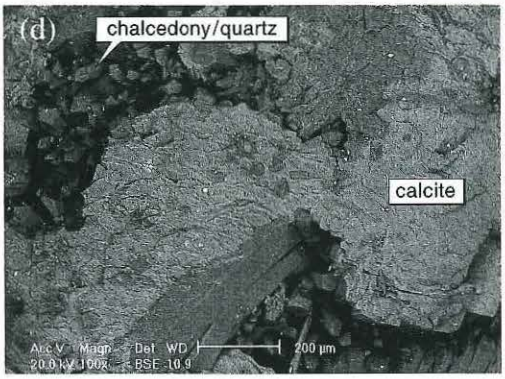

Fig. 8. (**a**) Core from a depth of 1308.8 m in the corehole K-33 showing the sinistral strike-slip fracture. The slip vector is defined by quartz. A silicified clay zone surrounds the fracture. Remnant dilatant regions of the fracture are filled by younger idiomorphic anhydrite precipitated from downward percolating condensate. (**b**) Core from a depth of 305.5 m in the corehole T-8 showing the tensile fracture. Fracture is lined by idiomorphic crystals of the older high-temperature epidote–chlorite–pyrite suite precipitated into the open space. A fractal of the remnant space was used for the precipitation of just one nest of the idiomorphic anhydrite. The remaining space remained open because there was no more condensate to feed the continuing filling of the space left. (**c**) Core from a depth of 2017.4 m in the corehole K-33 with a normal fracture with several dilatant regions. Dilatant regions are lined with the earlier pyrite and sealed by the younger calcite that precipitated from downward percolating condensate. (**d**) Scanning electron microscope (SEM) backscattered electron image with a vein filled by the earlier chalcedonic quartz and younger calcite from a depth of 794 m in the corehole T-2. Calcite fills the remaining space in the vein.

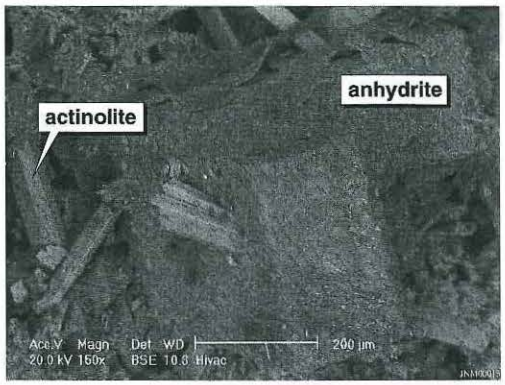

Fig. 9. SEM backscattered electron image of the vein from a depth of 1044.9 m in the corehole T-8 (Moore *et al.* 2000). Image shows the anhydrite crystals post-dating actinolite crystals. Subhorizontally oriented anhydrite crystal is coated with peeling-off titanium-rich scale, which indicates extremely dry conditions.

Fracture development within the geothermal system – interpretation and discussion

Liquid-dominated stage

Fractures of this stage are either newly formed or reactivated pre-existing fractures developed in the country rock. Our data (Table 1, Fig. 6b, 6e) suggest that these fractures were controlled by the stress regime, which was a result of plate movements, gravity forces and pore fluid pressures. The stress regime, with horizontal σ_1 and σ_3 stresses trending roughly N–S and E–W, respectively, controlled shear and tensile fractures in the shallow portion of the system. In the deeper portion of the system, σ_1 was vertical, whereas σ_3 was horizontal and roughly E–W trending. Cycles of fluid overpressure are indicated by implosion breccias (Fig. 6b), subhorizontal tensile fractures and anastomosing patterns of hydraulic fractures (Fig. 6e). Subhorizontal tensile fractures indicate that the fluid pressure was approaching the value of the effective overburden load. Implosion breccias indicate rapid bursts of fluid flow immediately post-failure, balancing fluid pressure gradients among various compartments of the fracture system. Random orientations of anastomosing tensile fracture patterns document fluid-assisted failure.

High pore fluid pressures, characteristic of this stage, were driven by the field-scale and local mechanisms. The field-scale mechanism involves a combination of a magmatic fluid source below the reservoir section and an effective cap rock above. Although the granodiorite underlying the geothermal system has not been dated directly, several lines of evidence indicate that the intrusion played a key role in the development of the liquid-dominated system. These include: (1) the presence of amphibole and epidote, which indicate temperatures in excess of 300 °C in rocks younger than 6000 years BP; (2) the simple vein parageneses suggesting a single major heating event; and (3) the parallelism of the isotherms with the intrusion geometry. Taken together, these relationships suggest that the initiation of the liquid-dominated system and the emplacement of the granodiorite occurred during the last 6000 years.

Magmatic fluids and gases can accumulate inside the magma column by a combination of the diffusion-driven fractionation (McBirney 1995 and references therein), compaction-driven fractionation (Shirley 1986, 1987; Sparks *et al.* 1985; Ortoleva *et al.* 1987)

and convection-driven fractionation (Tait *et al.* 1984; Morse 1986; Tait & Kerr 1987; Shinohara *et al.* 1995). Fluids released from magma can have a volume much larger than the volume of the intrusion itself. These volume relationships are demonstrated, for example, by mass-balance calculations made for the Pine Grove ore deposit, Colorado (Keith & Shanks 1988).

Our observations indicate that the cap rock initially consisted of permeable tuffs, pyroclastic and epiclastic horizons intercalated with impermeable lava flows.

The tuffs could have had initial porosities as high as 22%, as indicated by rock data compiled by Lama & Vutukuri (1978). This would have made them good reservoir rocks prior to their alteration and compaction. We do not have porosity data for the pyroclastic and epiclastic rocks, but their densities of approximately 2360 kg m^{-3} compared with lava flow densities of about 2430 kg m^{-3} indicate higher porosities than those of andesitic lava flows. As with the tuffs, the pyroclastic and epiclastic rocks were prone to penetrative shallow argillic alteration, and later compaction, which progressively changed them into effective seals during the liquid-dominated stage.

Unfractured brittle lava flows are sandwiched among the less competent tuffs, pyroclastic flows and epiclastic deposits. The lava flows initially formed seals inside the porous horizons. These flows show little alteration, indicating that the matrix porosity was too low to host the early penetrative fluids. Rock mechanics analogues (e.g. Lama & Vutukuri 1978) indicate an initial porosity of 8% or less for andesitic lava flows. The surrounding porous horizons absorbed the deformation, allowing lava flows to escape fracturing and retain their sealing properties.

Local-scale mechanisms capable of generating high fluid pressures include (e.g. Fournier 1967, 1999; Cunningham 1978; Byerlee 1993):

- fault self-sealing due to cementation combined with compaction, resulting in overpressured compartments;
- development of fractured zones sealed by incompetent horizons with porosity destroyed by alteration;
- boiling of upward migrating fluids, resulting in rapid volume expansion.

Observed textural relationships indicate that all three mechanisms operated. Evidence for the first mechanism is documented in Figure 6e. Here, fracture sealing by quartz cementation was followed by re-opening of the fracture and re-cementation by quartz. Self-sealing combined with compaction could have occurred in faults with horizontal component of displacement. Their cores are formed by tectonic gouge produced by cataclasis (Figure 6c). Conductive electric images of some of the cores (Christensen *et al.* 2002) indicate fluid saturation. Their cores are locally silicified and have rather irregular geometries. These complex geometries can result in the occurrence of local restraining bends, which lead to compaction, and to local releasing bends, which lead to dilation (e.g. Nur & Booker 1972; Segall & Pollard 1980; Sibson 1985, 1989). The presence of different deformation domains within the observed fault zones could have produced a complex system of pore fluid pressure gradients before faulting and their rapid equilibration during faulting (e.g. Muir Wood & King 1993; Muir Wood 1994).

There are frequent instances for the second mechanism in corehole K-33. The presence of incompetent horizons with porosity destroyed by alteration is shown in Figure 4. These horizons are significantly less affected by fracturing than the intercalated layers of brittle lava flows. They act as effective seals among the more fractured horizons, separating the rock section into numerous compartments with different pore fluid pressures. A similar behaviour occurs in multilayer sedimentary sequences (e.g. Nemčok *et al.* 1995, 2002).

There is abundant evidence for boiling. The core material from K-33 reveals that numerous fractures contain blade-shaped calcite crystals, which indicate boiling. The separation of the vapour phase during boiling results in rapid volume expansion.

Transition to vapour-dominated stage

The transition to vapour-dominated conditions was marked in the fractures by the deposition of chalcedony (Table 2). The presence of chalcedony throughout the reservoir at temperatures exceeding 235 °C implies extreme supersaturation of silica with respect to quartz. As discussed by Fournier (1985), catastrophic depressurization and boiling is the most likely cause of silica supersaturation at these temperatures. In T-8, rocks containing chalcedony overlie organic-bearing lake beds dated at 5910 ± 76 BP (Moore *et al.* 2002). However, no massive volcanic eruptions that could have depressurized the system are known to have occurred during the last 6000 years and the absence of older episodes of chalcedony implies that earlier volcanic eruptions were also of insufficient magnitude to cause extensive silica supersaturation and widespread boiling. We therefore conclude that depressurization must have been caused by the flank collapse that led to the formation of the volcano's crater, Kawah Galunggung at 4200 years BP (Bronto 1989). We suggest that this collapse was triggered by a combination of increased pore fluid pressures

and penetrative alteration, initiated during the liquid-dominated stage. Elevated N_2/Ar ratios of fluid inclusions trapped in quartz overprinting chalcedony in T-2, T-8 and K-33, combined with the high $^3He/^4He$ ratios of the modern gases and the oxygen isotope shifted compositions of the deep liquids, imply that the granodiorite continued to provide heat and fluids during the transition and later stages of the geothermal system's evolution.

Flank collapse must have been a major venting event for accumulated pore fluid pressures. The data described earlier demonstrate that chalcedony precipitation took part preferentially along steeply dipping fractures with the largest possible apertures. The orientations of these fractures indicate that the escaping overpressured fluids used the shortest possible paths to the surface. The choice of the shortest paths documents a rapid post-failure fluid redistribution.

The modern geothermal system

The fluid inclusion and mineral record demonstrates that vapour-dominated conditions were initiated following the transitional stage. As the vapour-dominated region expanded, the condensate that formed at the top of the steam zone percolated downward, modifying the cap rock–reservoir boundary. Anhydrite, calcite and pyrite were deposited as the fluids were heated. Figure 8a–d documents the downward shift of the cap rock–reservoir boundary caused by mineral deposition in the fractures. Although voids are present in the cap rock, thermal profiles (Fig. 1c) are indicative of conductive gradients and low overall permeabilities. The top of the present-day reservoir is indicated by the first occurrence of fractures with interconnected voids (Fig. 8b).

Some of the reservoir fractures have large cavities preserved in their dilatant areas (Figs 3c and 8b). Closed parts of reservoir fractures are formed by rock–rock or cemented rock–rock contacts, which support the open space among them against collapse. Locally, the open fractures are propped by breccias, which contain large voids among the clasts. Propping breccias support residual fracture apertures, but the average residual fracture porosity remains significant.

There is no evidence for pore fluid pressures equal or higher than hydrostatic in fractures within the vapour-dominated zone. Fractures related to the modern system do not contain implosion breccias or anastomosing offshoots. The fracturing in the geothermal system is now driven only by tectonic stresses and gravity. Pore fluid pressure is no longer capable of shifting the differential stress towards the failure envelope. Stress build-ups are driven only by plate motions interplaying with overburden changes due to new volcanic eruptions or erosion.

The liquid reservoir underlying the vapour-dominated zone is underpressured by several tens of bars relative to the surrounding regional groundwater system (Allis *et al.* 2000). During the time between reservoir fracture events, the residual fracture apertures were supported only by rock asperities or propping breccias. There is no evidence for increased pore fluid pressure to support the fracture apertures. Therefore, we conclude that the base of the fractured reservoir is controlled by the value of the normal stress acting on fracture walls. If it exceeds the compressive strength of asperities or propping breccias, collapse of the fractures will occur.

Rock mechanics data (e.g. Lama & Vutukuri 1978) indicate that porosity and density of andesitic lava flows are about 8% and 2430 kg m^{-3}, respectively. The porosity of andesitic tuffs is higher at about 22% and their density slightly lower at about 2160 kg m^{-3}. There are no data on porosities of andesitic epiclastic and pyroclastic rocks, but their average density of about 2360 kg m^{-3} indicates a higher porosity than that of andesitic lava flows. The average density of a sandy tuff is 1910 kg m^{-3}, suggesting even higher porosities. These data are consistent with the observation that fluid entries in lava flows and pyroclastics are fracture controlled. In contrast, there is a lack of fractures associated with fluid entries in the more porous epiclastic and tuff deposits. Fluid entries in these zones are controlled by high matrix permeabilities. Fracture permeability thus competes with matrix permeability in the reservoir. It dominates in massive and low permeability volcanic sequences, whereas it is subordinate in the more porous layered volcanoclastic and sedimentary sections.

Conclusions

- The stress field during the development of the Karaha–Telaga Bodas geothermal system has remained relatively stable. Fractures in the cap rock have been controlled by a strike-slip stress regime. The orientations of the principal stresses are $\sigma_1 = 188°/0°$, $\sigma_2 = 0°/90°$ and $\sigma_3 = 98°/0°$. Fractures in the reservoir have been controlled by the extensional stress regime. The orientations of the principal stresses are $\sigma_1 = 0°/90°$, $\sigma_2 = 188°/0°$ and $\sigma_3 = 98°/0°$.
- The fracture system within the geothermal field consists mainly of normal faults and tensile fractures with strikes of 350°–30° and dextral strike-slip faults with strikes of 120°–140°. Other less numerous sets include sinistral oblique-slip faults with strikes of 30°–40°, sinistral strike-slip faults with strikes of 50°–70° and dextral

oblique-slip faults with strikes of 140°–170°. Productive fractures are steep and have strikes around 8°, although large productive faults with different orientations are present. Their size apparently makes up for their less favourable orientation.

- Conductive temperature profiles characterize the cap rock, whereas the reservoir is characterized by convective profiles. The cap rock consists of penetratively deformed horizons of incompetent rocks and competent rocks with poorly connected fracture systems. Sealed fractures are cemented by calcite, quartz and anhydrite. Productive fractures within the reservoir are characterized by large interconnected voids located in dilatant regions. These voids are supported by rock asperities, cement bridges or propping breccias.
- The geothermal system developed rapidly within the last 6000 years. Three stages in its development can be recognized.

The earliest stage was liquid-dominated. It is characterized by penetrative alteration that enhanced the cap rock. Fracturing was controlled by tectonic stress interacting with the overburden load and modified by pore fluid pressures. Cooling-related residual-stress development contributed to this control only locally. Pore fluid pressures above hydrostatic locally developed and were driven by interacting mechanisms such as fault–fracture compaction, fault–fracture cementation, and input of magmatic fluids and magmatic heating.

Stage 2 represents the transition from the liquid- to a vapour-dominated stage. It is characterized by a catastrophic drop in pore fluid pressure, triggered by a flank collapse of Galunggung volcano 4200 years ago. Chalcedony and quartz were deposited in fractures with the shortest possible path to the surface. Fracturing was strongly affected by pore fluid pressures.

Stage 3 represents the modern vapour- and deep liquid-dominated regimes. The liquid represents the inflow of low-salinity meteoric waters. Fracturing during this stage was driven by the tectonic stress interacting with the overburden load. There was no evidence for high pore fluid pressures. Precipitation from condensed vapour progressively sealed the fracture system downwards, resulting in expansion of the cap rock. Pore fluid pressures are below hydrostatic in the modern reservoir. Fractures have collapsed to their residual apertures, supported only by rock asperities, cement bridges and propping breccias. The normal stress acting upon the fracture walls controls the base of the productive reservoir. The fracture apertures collapse completely where normal stresses exceed the compressive strength of the host rock.

M. Nemčok and J. N. Moore were supported by DOE grants to EGI (01-0059-5000-55800164 and 01-0059-5000-55900160). The management and staff of the Karaha–Bodas Company are thanked for providing data in support of this research. Authors wish to thank D. Jensen for help with drafting, and K. M. Kovac and S. Moore for help with editing. The final version of the paper was considerably improved by constructive criticism from A. Gudmundsson.

References

ADAMS, J. T. & DART, C. 1998. The appearance of potential sealing faults on borehole images. *In*: JONES, G., FISHER, Q. J. & KNIPE, R. J. (eds) *Faulting, Fault Sealing and Fluid Flow in Hydrocarbon Reservoirs*. Geological Society, London, Special Publications, **147**, 71–86.

ALLIS, R. & MOORE, J. N. 2000. Evolution of volcano-hosted vapor-dominated geothermal systems. *Geothermal Resources Council Transactions*, **24**, 24–27.

ALLIS, R., MOORE, J.N., MCCULLOCH, J., PETTY, S. & DEROCHER, T., 2000. Karaha–Telaga Bodas, Indonesia: a partially vapor-dominated geothermal system. *Geothermal Resources Council Transactions*, **24**, 217–222.

ANTONELLINI, M. & AYDIN, A. 1994. Effect of faulting on fluid flow in porous sandstones: Petrophysical properties. *AAPG Bulletin*, **78**, 355–377.

BARTON, C. A., ZOBACK, M. D. & MOOS, D. 1995. Fluid flow along potentially active faults in crystalline rock. *Geology*, **23**, 683–686.

BAUMANN, P. 1982. Depositional cycles on magmatic and back arcs; an example from western Indonesia. *Revue de l'Institut Francais du Petrole*, **37**, 3–17.

BLANPIED, M. L., LOCKNER, D. A. & BYERLEE, J. D. 1995. Frictional slip of granite at hydrothermal conditions. *Journal of Geophysical Research*, **100**, 13045–13064.

BOTT, M. H. P. 1959. The mechanics of oblique slip faulting. *Geological Magazine*, **96**, 109–117.

BRANTLEY, S. & GLICKEN, H. 1986. Volcanic debris avalanches. *In*: *Earthquakes and Volcanoes*. US Geological Survey Report, EV, **5**, 195–206.

BRONTO, S. 1989. *Volcanic geology of Galunggung, West Java, Indonesia*. PhD thesis, University of Canterbury.

BUDHITRISNA, T. 1986. *Peta Geologi Lembar Tasikmalaya, Jawa Barat*, scale 1:100000. Pusat Penelitian Dan Pengembangan Geologi.

BYERLEE, J. 1993. Model for episodic flow of high-pressure water in fault zones before earthquakes. *Geology*, **21**, 303–306.

CAPPETTI, G., CELATI, R., CIGNI, U., SQUARCI, P., STEFANI, G. & TAFFI, L. 1985. Development of deep exploration in the geothermal areas of Tuscany, Italy. *In*: STONE, C. (ed.) *International Symposium on Geothermal Energy, International Volume*. Geothermal Resources Council, Davis, CA, 303–309.

CHRISTENSEN, C., NEMČOK, M., MCCULLOCH, J. & MOORE, J. 2002. The characteristics of productive zones in the Karaha–Telaga Bodas geothermal system.

Geothermal Resources Council Transactions, **26**, 623–626.

CUNNINGHAM, C. G. 1978. Pressure gradients and boiling mechanisms for localizing ore in porphyry systems. *US Geological Survey Journal of Research*, **6**, 745–754.

ENGELDER, T. & FISCHER, M. P. 1994. Influence of poroelastic behavior on the magnitude of minimum horizontal stress, S_h, in overpressured parts of sedimentary basins. *Geology*, **22**, 949–952.

ETHERIDGE, M. A. 1983. Differential stress magnitudes during regional deformation and metamorphism: Upper bounds imposed by tensile fracturing. *Geology*, **11**, 231–234.

FERRARA, G. C., PALMERINI, G. C. & SCAPPINI, U. 1985. Update report on geothermal development in Italy. *In*: STONE, C. (ed.) *International Symposium on Geothermal Energy, International Volume.* Geothermal Resources Council, Davis, CA, 95–105.

FOURNIER, R. O. 1985. The behavior of silica in hydrothermal solutions. *In*: BERGER, B. R. & BETHKE, P. M. (eds) *Geology and Geochemistry of Epithermal Systems. Reviews in Economic Geology*, **2**, 45–61.

FOURNIER, R. O. 1991. The transition from hydrostatic to greater than hydrostatic fluid pressure in presently active continental hydrothermal systems in crystalline rock. *Geophysical Research Letters*, **18**, 955–958.

FOURNIER, R. O. 1999. Hydrothermal processes related to movement of fluid from plastic into brittle rock in the magmatic–epithermal environment. *Economic Geology*, **94**, 1193–1212.

GANDA, S., BOEDIHARDI, M., RACHMAN, A. & HANTONO, D. 1985. *Geologi daerah Kawah dan Sekitarnyia Kabupaten Tasikmalaya, Garut, Majalengka dan Sumedang, Proponsi Jawa Barat.* Divisi Geotermal, Pertamina Pusat.

GILPIN, B. & LEE, T. C. 1978. A microearthquake study of the Salton Sea geothermal area, California. *Seismological Society of America Bulletin*, **68**, 441–450.

HALL, R. 1997. Cenozoic tectonics of SE Asia and Australasia. *In*: HOWES, J.V.C. & NOBLE, R.A. (eds) *Proceedings of an International Conference on Petroleum Systems of SE Asia and Australasia, Jakarta, Indonesia, 21–23 May 1997.* Indonesian Petroleum Association, Jakarta, 47–62.

HALLIBURTON, 1995. *Electrical Micro Imaging Service, Brochure, EL1076.*

HAMILTON, W. 1974*a*. *Earthquake Map of the Indonesian Region.* Department of the Interior, US Geological Survey, Reston.

HAMILTON, W. 1974*b*. *Map of Sedimentary Basins of the Indonesian Region.* Department of the Interior, US Geological Survey, Reston.

HAMILTON, W. 1978. *Tectonic map of the Indonesian Region.* Department of the Interior, US Geological Survey, Reston.

HARDEBECK, J. L. & HAUKSSON, E. 1999. Role of fluids in faulting inferred from stress field signatures. *Science*, **285**, 236–239.

HEDENQUIST, J. W., ARRIBAS, A., JR & REYNOLDS, T. J. 1998. Evolution of an intrusion–centered hydrothermal system: Far Southeast-Lepanto porphyry and epithermal Cu–Au deposits, Philippines. *Economic Geology*, **93**, 373–404.

HENLEY, R. W. & ELLIS, A. J. 1983. Geothermal systems ancient and modern; a geochemical review. *Earth-Science Reviews*, **19**, 1–50.

KATILI, J. A. & SUDRADJAT, A. 1984. *Galunggung: the 1982–83 Eruption.* Volcanological Survey of Indonesia, Bandung, 102.

KEITH, J. D. & SHANKS, W. C. 1988. Chemical evolution and volatile fugacities of the Pine Grove porphyry molybdenum and ash-flow tuff system, southwestern Utah. *In*: TAYLOR, R. P. & STRONG, D. F. (eds) *Recent Advances in the Geology of Granite-related Mineral Deposits.* Canadian Institute of Mining and Metallurgy, Special Volume, **39**, 402–423.

LAMA, R. D. & VUTUKURI, V. S. 1978. *Handbook on Mechanical Properties of Rocks.* Transtech Publications, Bay Village.

MAJER, E. L. & MCEVILLY, 1979. Seismological investigation at The Geysers geothermal field. *Geophysics*, **44**, 246–269.

MALIN, P. 1994. The seismology of extensional hydrothermal system. *Geothermal Resources Council Transactions*, **18**, 17–22.

MANDL, G. 1988, *Mechanics of Tectonic Faulting. Models and Basic Concepts.* Elsevier, Amsterdam.

MCBIRNEY, A. R. 1995. Mechanisms of differentiation in the Skaergaard intrusion. *Journal of Geological Society, London*, **152**, 421–435.

MILLER, S. A., NUR, A. & OLGAARD, D. L. 1996. Earthquakes as a coupled shear stress – high pore pressure dynamical system. *Geophysical Research Letters*, **23**, 197–200.

MOORE, J. N., ALLIS, R. G. & MCCULLOCH, J. E. 2001. The origin and development of vapor-dominated geothermal systems. *In*: *Eleventh Annual V.M. Goldschmidt Conference, 20–24 May 2001, Hot Springs, Virginia, USA.* Lunar and Planetary Institute, Houston, TX.

MOORE, J. N., CHRISTENSEN, B., BROWNE, P. R. L. & LUTZ, S. J. 2004. The mineralogic consequences and behavior of descending acid-sulfate waters: an example from the Karaha–Telaga Bodas geothermal system, Indonesia. *Canadian Mineralogist* (in press).

MOORE, J. N., LUTZ, S. J., RENNER, J. L., MCCULLOCH, J. & PETTY, S. 2000. Evolution of a volcanic-hosted vapor-dominated system: petrologic and geochemical data from corehole T-8, Karaha–Telaga Bodas, Indonesia. *Geothermal Resources Council Transactions*, **24**, 24–27.

MOORE, J. N., ALLIS, R. G., RENNER, J., MILDENHALL, D. & MCCULLOCH, J. 2002. Petrologic evidence for boiling to dryness in the Karaha–Telaga Bodas geothermal system, Indonesia. *In*: *Proceedings of the 27th Stanford Workshop on Geothermal Reservoir Engineering, 28–30 January 2002.* Stanford University, Stanford, CA, 223–232.

MORSE, S. A. 1986. Convection in aid of adcumulus growth. *Journal of Petrology*, **27**, 1183–1214.

MUELLER, B., WEHRLE, V. & FUCHS, K. 1997. The 1997 release of the World Stress Map. http://www-wsm.physik.uni-karlsruhe.de/pub/Rel97/wsm97.html.

MUIR WOOD, R. 1994. Earthquakes, strain-cycling and the mobilization of fluids. *In*: PARNELL J. (ed.) *Geofluids; Origin, Migration and Evolution of Fluids in Sedimentary Basins.* Geological Society, London, Special Publications, **78**, 85–98.

MUIR WOOD, R. & KING, G. C. P. 1993. Hydrological signatures of earthquake strain. *Journal of Geophysical Research*, **98**, 22035–22068.

MURASE, T. & MCBIRNEY, A. R. 1973. Properties of some common igneous rocks and their melts at high temperatures. *Geological Society of America Bulletin*, **84**, 3563–3592.

NEMČOK, M., GAYER, R. A. & MILIORIZOS, M. 1995. Structural analysis of the inverted Bristol Channel Basin: Implications for the geometry and timing of the fracture porosity. *In*: BUCHANAN, J. G. & BUCHANAN, P. G. (eds) *Basin Inversion*. Geological Society, London, Special Publications, **82**, 355–392.

NEMČOK, M., HENK, A., GAYER, R. A., VANDYCKE, S. & HATHAWAY, T. M. 2002. Strike-slip fault bridge fluid pumping mechanism: insights from field-based palaeostress analysis and numerical modelling. *Journal of Structural Geology*, **24**, 1885–1901.

NEMČOK, M., MCCULLOCH, J., NASH, G & MOORE, J. N. 2001. Fault kinematics in the Karaha-Telaga Bodas, Indonesia, geothermal field: an interpretation tool for remote sensing data. *Geothermal Resources Council Transactions*, **25**, 26–29.

NUR, A. & BOOKER, J. R. 1972. Aftershocks caused by pore fluid flow? *Science*, **175**, 885–887.

ORTOLEVA, P., MERINO, E., MOORE, C. & CHADAM, J. 1987. Geochemical self-organization, I. Reaction-transport feedbacks and modeling approach. *American Journal of Science*, **287**, 979–1007.

POWELL, T., MOORE, J., DEROCHER, T. & MCCULLOCH, J. 2001. Reservoir geochemistry of the Karaha–Telaga Bodas prospect, Indonesia. *Geothermal Resources Council Transactions*, **24**, 363–367.

RENNER, J., EVANS, B. & HIRTH, G. 2000. On the rheologically critical melt fraction. *Earth and Planetary Science Letters*, **181**, 585–594.

RICE, J. & CLEARY, M. 1976. Some basic stress diffusion solutions for fluid-saturated elastic porous media with compressible constituents. *Reviews of Geophysics and Space Physics*, **14**, 227–241.

SCHLUMBERGER, 1992. *FMI Fullbore Micro Imager, Brochure SMP 9210*.

SECOR, D. T. 1965. Role of fluid pressure in jointing. *American Journal of Science*, **263**, 633–646.

SEGALL, P. & POLLARD, D. D. 1980. Mechanics of discontinuous faults. *Journal of Geophysical Research*, **85**, 4337–4350.

SHAW, H. R. 1969. Rheology of basalt in the melting range. *Journal of Petrology*, **10**, 510–535.

SHINOHARA, H., KAZAHAYA, K. & LOWENSTERN, J. B. 1995. Volatile transport in a convecting magma column: Implications for porphyry Mo mineralization. *Geology*, **23**, 1091–1094.

SHIRLEY, D. N. 1986. Compaction of igneous cumulates. *Journal of Geology*, **94**, 795–809.

SHIRLEY, D. N. 1987. Differentiation and compaction in the Palisades Sill. *Journal of Petrology*, **28**, 835–865.

SIBSON, R. H. 1982. Fault zone models, heat flow, and the depth distribution of seismicity in the continental crust of the United States. *Seismological Society of America Bulletin*, **72**, 151–163.

SIBSON, R. H. 1985. Stopping of earthquake ruptures at dilational fault jogs. *Nature*, **316**, 248–251.

SIBSON, R. H. 1989. Earthquake faulting as a structural process. *Journal of Structural Geology*, **11**, 1–14.

SIBSON, R. H. 1996. Structural permeability of fluid-driven fault-fracture meshes. *Journal of Structural Geology*, **18**, 1031–1042.

SPARKS, R. S. J., HUPPERT, H. E., KERR, R. C., MCKENZIE, D. P. & TAIT, S. R. 1985. Postcumulus processes in layered intrusions. *Geological Magazine*, **122**, 555–568.

TAIT, S. R. & KERR, R. C. 1987. Experimental modelling of interstitial melt convection in cumulus piles. *In*: PARSON, I. (ed.), *Origins of Igneous Layering*. NATO ASI Series C, **196**, 569–587.

TAIT, S. R., HUPPERT, H. E. & SPARKS, R. S. J. 1984. The role of compositional convection in the formation of adcumulate rocks. *Lithos*, **17**, 139–146.

TSANG, C. F. 1999. Linking thermal, hydrological, and mechanical processes in fractured rocks. *Annual Reviews of Earth and Planetary Sciences*, **27**, 359–384.

WALLACE, R. E. 1951. Geometry of shearing stress and relation to faulting. *Journal of Geology*, **59**, 118–130.